

See discussions, stats, and author profiles for this publication at: <https://www.researchgate.net/publication/8008608>

Mn-55 pulse ENDOR at 34 GHz of the S-0 and S-2 states of the oxygen-evolving complex in photosystem II

ARTICLE *in* JOURNAL OF THE AMERICAN CHEMICAL SOCIETY · APRIL 2005

Impact Factor: 12.11 · DOI: 10.1021/ja043012j · Source: PubMed

CITATIONS

121

READS

26

4 AUTHORS, INCLUDING:



Leonid Kulik

Russian Academy of Sciences

56 PUBLICATIONS 893 CITATIONS

SEE PROFILE



Boris Epel

University of Chicago

69 PUBLICATIONS 1,036 CITATIONS

SEE PROFILE

⁵⁵Mn Pulse ENDOR at 34 GHz of the S₀ and S₂ States of the Oxygen-Evolving Complex in Photosystem II

Leonid V. Kulik,[§] Boris Epel, Wolfgang Lubitz,* and Johannes Messinger*

Max-Planck-Institut für Bioanorganische Chemie, Stiftstrasse 34-36, D-45470 Mülheim/Ruhr, Germany

Received November 19, 2004; E-mail: lubitz@mpi-muelheim.mpg.de; messinger@mpi-muelheim.mpg.de

Powered by light-induced charge separations that generate oxidizing equivalents of about +1.3 V, photosystem II (PSII) has the unique capability to oxidize water to molecular oxygen. Water splitting is catalyzed by a Mn₄O_xCa complex housed in a special protein environment that also controls proton movements and the access of water. This functional unit of PSII is referred to as the oxygen-evolving complex (OEC). PSII created the aerobic atmosphere on earth and may serve as a model for technical approaches to split water by sunlight, which is a prerequisite for a sustainable hydrogen economy. Despite the availability of crystal structures of PSII with 3.5 and 3.2 Å resolutions and of extensive EPR and EXAFS studies, the precise geometric and electronic structures of the various functional states of the Mn₄O_xCa complex are still unknown.^{1–5} During the reaction sequence (Kok cycle) the OEC passes through five oxidation states (S states, S₀–S₄),⁶ of which the S₀ and S₂ states have $S = 1/2$ ground states. Continuous wave (CW) EPR has been used to study the electronic structures of these states,^{7–10} but despite the rich hyperfine structures of the S₂ and S₀ EPR multiline signals, it has not been possible to uniquely determine the hyperfine interaction (HFI) tensors of the individual Mn ions in this way. For such complex spin systems, it is required to directly probe the Mn HFI parameters by ⁵⁵Mn pulse ENDOR spectroscopy. For technical reasons and due to the complex preparation procedure for concentrated S₀ state samples, such experiments were done so far only at X-band for the S₂ state; they gave the first reliable HFI parameters.¹¹ In this study we report ⁵⁵Mn pulse ENDOR spectra for the S₀ and S₂ states at Q-band frequency (34 GHz). Numerical analysis of our spectra (i) shows that all four Mn ions are magnetically coupled, (ii) allows a refinement of the HFI parameters for the S₂ state, (iii) provides the first reliable HFI tensors for the S₀ state, and (iv) leads to a suggestion for the Mn oxidation states in S₀ and S₂.

PSII membranes were prepared according to standard procedures⁸ and washed several times after the Triton treatment to completely remove starch. S₂ state samples were obtained by concentrating dark-adapted PSII membranes containing 250 μM PPBQ (phenyl-*p*-benzoquinone) and 1 mM EDTA in 3 mm quartz tubes by centrifugation (~25 mg of chlorophyll/mL final) and subsequent 200 K illumination. S₀ state samples were prepared using the three-flash/FCCP approach described previously.^{8,12} The samples were finally concentrated by centrifugation in the Q-band EPR tubes. After completion of the ⁵⁵Mn ENDOR experiments, the S₀ state population was determined to be 65 ± 5% (the rest being S₁) on the basis of the amplitude of the S₂ EPR multiline signal generated by 200 K illumination compared to that of S₂ control samples. All samples contained 3% (v/v) methanol.

The experiments were performed on a Bruker ESP-580 Q-band pulse EPR spectrometer equipped with a home-built ENDOR cavity. The pulse ENDOR experiments were performed using SpecMan

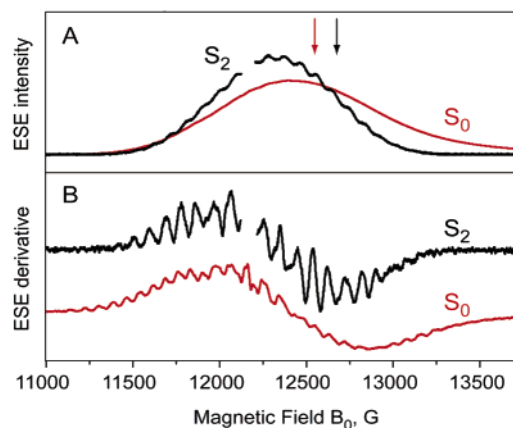


Figure 1. Q-band echo-detected EPR spectra (light minus dark) of the S₂ and S₀ states (A) and their numerical pseudomodulation with 20 G amplitude, which gives CW EPR-like derivative spectra (B). $T = 4.5$ K, mw $\pi/2$ -pulse 32 ns, $\tau = 260$ ns, $\nu_{mw} = 33.850$ GHz (S₂ state), 34.123 GHz (S₀ state). The spectra of the S₂ state are shifted by 100 G to higher magnetic field to compensate for the mw frequency difference. The pulse repetition time was 1 ms (S₂ state) and 12 μs (S₀ state). The arrows indicate the magnetic field positions where ⁵⁵Mn ENDOR spectra were taken (see Figure 2). In the S₂ state spectra, the sharp signal of the tyrosine D radical of PSII at $g \approx 2$ is removed for clarity. This signal is practically absent for the S₀ state sample due to chemical reduction by FCCP.

control software that varies the radio frequency (rf) randomly in the desired range. This leads to a decrease of the rf-induced heat accumulation in the resonator and in turn to a reduction of heating artifacts.

Figure 1A shows the two-pulse echo-detected EPR spectra of the S₂ and S₀ states (light minus dark difference). A comparison reveals that the S₀ signal is ~500 G broader and that the extra width mainly stems from the high-field wing. This indicates substantial g -anisotropy in the S₀ state and shows that g_{iso} of the S₀ state is smaller than g_{iso} of the S₂ state. The CW EPR-like derivative spectra of Figure 1B are produced by numerical pseudomodulation of the field sweeps (Figure 1A) using a 20 G amplitude. This procedure allows a closer inspection of the hyperfine structure. For the S₀ state, this is the first report of a CW-like Q-band EPR spectrum. The total width is about 2500 G, and at least 26 lines are resolved. At the low-field side the average splitting is about 78 G, and at the high-field side it is 84 G. The overall similarity to the well-known S₀ state CW EPR X-band spectrum confirms that the Q-band two-pulse echo originates from the S₀ state. An inversion–recovery measurement of the spin lattice relaxation time T_1 for the S₀ state (data not shown) gives $T_1 \approx 9$ μs at 4.5 K, which is about 100 times faster than the T_1 of the S₂ state.¹³ This is in line with previous reports that the S₀ state has a higher half-saturation power than the S₂ state.^{9,14}

The black lines in Figure 2 show the ⁵⁵Mn ENDOR spectra of the S₂ and S₀ states that were recorded at the magnetic field

[§] Permanent address: Institute of Chemical Kinetics and Combustion, Institutskaya 3, 630090 Novosibirsk, Russia.

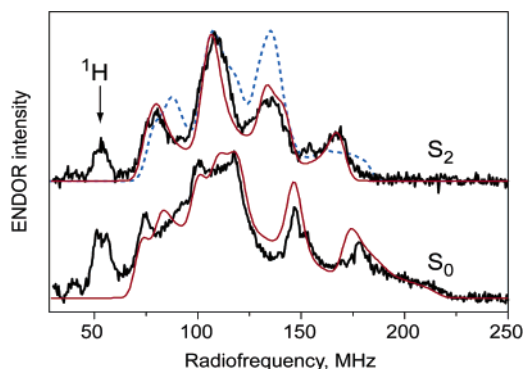


Figure 2. ^{55}Mn pulse ENDOR spectra at Q-band of the S_2 and S_0 states (black) and simulations using either the parameters of Table 1 (red) or those determined previously by Pelouin et al.¹¹ on the basis of X-band ^{55}Mn ENDOR (broken blue line). The Davies ENDOR sequence was used with a radio frequency (rf) π -pulse duration of 5 μs (S_2 state) and 4 μs (S_0 state). Temperature and other conditions are the same as in Figure 1. $B_0 = 12600$ G (S_2 state) and 12550 G (S_0 state).

Table 1. Principal Values of HFI Tensors (Absolute Values) of Individual ^{55}Mn Ions Used for Simulation of the ^{55}Mn ENDOR Spectra of the OEC

	S_2 state		S_0 state	
	A_{\perp} , MHz	A_{\parallel} , MHz	A_{\perp} , MHz	A_{\parallel} , MHz
Mn_A	235	265	270	200
Mn_B	185	245	190	280
Mn_C	310	265	320	400
Mn_D	175	230	170	240

positions indicated by the arrows in Figure 1A. Similar results were obtained at other field positions, which indicates a negligible orientation selection (data not shown). The S_2 state spectrum spans from 70 to 180 MHz, which is 20 MHz wider than at X-band. This difference is readily explained by the increased Zeeman frequency of the Mn nuclei (13 MHz at Q-band vs 3 MHz at X-band). The spectrum of the S_0 state is broader than that of the S_2 state; a weak shoulder extends to 220 MHz. Its low-frequency edge is probably at 70 MHz, but there is the possibility that a weak wing spans below the proton peak down to ~ 50 MHz. Scans up to 400 MHz do not reveal any additional signals.

Because of the small orientation selection, the mean ^{55}Mn ENDOR frequency (the “center of gravity” of the spectrum) equals approximately half of the absolute value of the isotropic Mn HFI constants averaged over the four Mn nuclei, $\langle |A_{\text{iso}}| \rangle / 2$. For theoretical spectra, this procedure has shown a precision of better than 1%. Analysis of the experimental ^{55}Mn ENDOR spectrum of the S_0 state gives $\langle |A_{\text{iso}}| \rangle = 250$ MHz. In the case of isotropic Mn HFI tensors, their contribution to the width of the EPR spectrum is $W_{\text{HFI}} = 5N\langle |A_{\text{iso}}| \rangle$, where N is the number of Mn nuclei. Any anisotropy in the HFI increases this value. The simulation shows that this increase is about 12% for the S_0 state (Table 1). The total width of the X-band S_0 state EPR spectrum is $W_{\text{T}} = 6160\text{--}6700$ MHz ($g = 2$).⁸ With $N = 4$, we obtain $W_{\text{HFI}} = 5600$ MHz. The difference between W_{HFI} and W_{T} can be explained by a g -tensor anisotropy of $\Delta g \approx 0.1\text{--}0.2$, which is in the expected range. A trinuclear or binuclear origin for the S_0 multiline requires a much larger g -tensor anisotropy of $\Delta g \approx 0.4\text{--}0.5$ or $0.65\text{--}0.75$, respectively. This strongly disfavors such proposals. For the S_2 state, the comparison of $W_{\text{T}} = 5400$ MHz and $W_{\text{HFI}} = 4700$ MHz (Q-band) gives an

upper limit of $\Delta g \approx 0.04$ for $N = 4$, which agrees with the previously reported values of $\Delta g \approx 0.02\text{--}0.04$.^{11,15} and further supports the idea that all four Mn nuclei are magnetically coupled in both states.

The red lines in Figure 2 show numerical simulations of the ^{55}Mn ENDOR spectra, performed using second-order perturbation theory.¹⁶ Only the allowed transitions were taken into account. For simplicity, axial g -tensors and Mn HFI tensors with coinciding directions for the symmetry axes were assumed, and Mn nuclear quadrupole interaction (NQI) was excluded (Table 1). Within this simple model, the precision of the simulation is ± 10 MHz. Since the signs of HFI constants cannot be determined by ENDOR simulations, only their absolute values are presented. We used $g_{\perp} = 1.97$, $g_{\parallel} = 1.99$ for the S_2 state and $g_{\perp} = 1.99$, $g_{\parallel} = 1.89$ for the S_0 state (see above). However, the simulated ^{55}Mn ENDOR spectrum is essentially insensitive to the variation of the principal values of the g -tensor. The HFI parameters for the S_2 state are close to those derived previously on the basis of X-band ^{55}Mn ENDOR; a simulation using these previously reported parameters is shown for visual comparison as the broken blue line in Figure 2.¹¹

Overall, surprisingly similar ^{55}Mn ENDOR spectra (Figure 2) and HFI parameters (Table 1) are found in this study for the S_0 and S_2 states. This appears to favor $\text{Mn}_4(\text{III}, \text{III}, \text{III}, \text{IV})$ and $\text{Mn}_4(\text{III}, \text{IV}, \text{IV}, \text{IV})$ as oxidation states for the S_0 and S_2 states, respectively, over alternative assignments that contain one Mn(II) in the S_0 state. This idea and possible structural models for the $\text{Mn}_4\text{O}_x\text{Ca}$ complex will be tested in a forthcoming publication, where the obtained HFI parameters will be used together with various spin-coupling schemes for the simulation of the hyperfine structures of the S_2 and S_0 EPR signals.

Acknowledgment. Leonid Kulik is grateful to the Alexander von Humboldt Foundation for financial support. This work was supported by the Max Planck Society and by the DFG (Me 1629/2-3).

References

- Messinger, J. *Phys. Chem. Chem. Phys.* **2004**, *6*, 4764–4771.
- Carell, T. G.; Tyryshkin, A. M.; Dismukes, G. C. *J. Biol. Inorg. Chem.* **2002**, *7*, 2–22.
- McEvoy, J. P.; Brudvig, G. W. *Phys. Chem. Chem. Phys.* **2004**, *6*, 4754–4763.
- Ferreira, K. N.; Iverson, T. M.; Maghlaoui, K.; Barber, J.; Iwata, S. *Science* **2004**, *303*, 1831–1838.
- Biesiadka, J.; Loll, B.; Kern, J.; Irrgang, K.-D.; Zouni, A. *Phys. Chem. Chem. Phys.* **2004**, *6*, 4733–4736.
- Kok, B.; Forbush, B.; McGloin, M. *Photochem. Photobiol.* **1970**, *11*, 457–476.
- Dismukes, G. C.; Siderer, Y. *Proc. Natl. Acad. Sci. U.S.A.* **1981**, *78*, 274–278.
- Messinger, J.; Robblee, J. H.; Yu, W. O.; Sauer, K.; Yachandra, V. K.; Klein, M. P. *J. Am. Chem. Soc.* **1997**, *119*, 11349–11350.
- Messinger, J.; Nugent, J. H. A.; Evans, M. C. W. *Biochemistry* **1997**, *36*, 11055–11060.
- Ahring, K. A.; Peterson, S.; Styring, S. *Biochemistry* **1997**, *36*, 13148–13152.
- Pelouin, J. M.; Campbell, K. A.; Randall, D. W.; Evanchik, M. A.; Pecoraro, V. L.; Armstrong, W. H.; Britt, R. D. *J. Am. Chem. Soc.* **2000**, *122*, 10926–10942.
- Robblee, J. H.; Messinger, J.; Cinco, R. M.; McFarlane, K. L.; Fernandez, C.; Pizarro, S. A.; Sauer, K.; Yachandra, V. K. *J. Am. Chem. Soc.* **2002**, *124*, 7459–7471.
- Lorigan, G. A.; Britt, R. D. *Biochemistry* **1994**, *33*, 12072–12076.
- Peterson, S.; Ahring, K. A.; Styring, S. *Biochemistry* **1999**, *38*, 15223–15230.
- Zheng, M.; Dismukes, G. C. *Inorg. Chem.* **1996**, *35*, 3307–3319.
- Sturgeon, B. E.; Ball, J. A.; Randall, D. W.; Britt, R. D. *J. Phys. Chem.* **1994**, *98*, 12871–12883.

JA043012J